JCTC Journal of Chemical Theory and Computation

Article

pubs.acs.org/JCTC

Quantum Chemical Free Energies: Structure Optimization and Vibrational Frequencies in Normal Modes

GiovanniMaria Piccini and Joachim Sauer*

Institut für Chemie, Humboldt Universität zu Berlin, Unter den Linden 6, Berlin, Germany

Supporting Information

ABSTRACT: A computational protocol is presented that uses normal mode coordinates for structure optimization and for obtaining harmonic frequencies by numerical differentiation. It reduces numerical accuracy problems encountered when density functional theory with plane wave basis sets is applied to systems with flat potential energy surfaces. The approach is applied to calculate Gibbs free energies for adsorption of methane, ethane, and propane on the Brønsted acidic sites of zeolite H−CHA. The values obtained (273.15 K, 0.1 MPa,), −0.25, −5.95, and −16.76 kJ/mol, respectively, follow the trend of the experimental values, which is not the case for results obtained with the standard approach (Cartesian optimization, frequencies from Cartesian distortions). Anharmonicity effects have been approximately taken into account by solving one-dimensional Schrödinger equations along each normal mode. This leads to a systematic increase of the Gibbs free energy of adsorption of 4.5, 5.0, and 3.1 kJ/mol for methane, ethane, and propane, respectively, making adsorption at a given pressure and temperature less likely. This is due to an increase of low vibrational frequencies associated with hindered translations and rotations of the adsorbed molecules and the floppy modes of the zeolite framework.

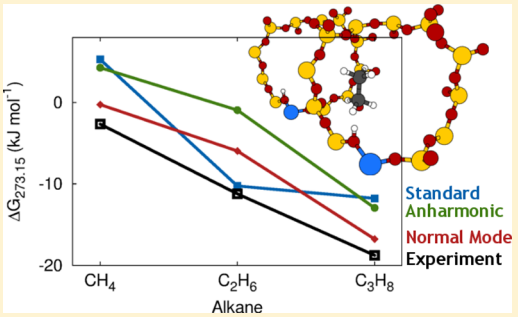

INTRODUCTION

Substantial progress has been made in calculating *ab initio* reaction energies in large chemical systems with chemical accuracy. Examples are the computation of energy barriers for enzymatic reactions[1] or for reactions in zeolite catalysts.[2−4] These calculations combine high level quantum chemical calculations for the reaction site with low level calculations of the periodic structure, either force fields[1] or density functional theory (DFT).[2−4]

The determination of rate and equilibrium constants that can be compared with experiments requires the calculation of free energy differences, i.e., entropies (see ref 5 for the important role of adsorption entropies). Unfortunately, entropy contributions to free energies presently cannot be calculated with the same accuracy. When force fields are available even for the quantum part of the above hybrid schemes, one of the available sampling schemes such as umbrella sampling[6] or thermodynamic integration[7] can be applied.[1] However, differently from biomolecular simulations, reliable force fields are rarely available for molecule−surface interactions involving active sites and the calculation of entropy contributions from vibrational partition functions evaluated in the harmonic approximation has become a standard tool to evaluate rate constants for surface reactions[3] and free energies of adsorption.[8−11] However, the numerical accuracy of calculated harmonic vibrational frequencies becomes a problem because the smallest frequencies make the largest contribution to the entropy and small numerical errors may have a large impact on the calculated entropies[12] (p 339, section 10.5.2). This has its origin in the exponential behavior of the vibrational entropy of an ideal harmonic solid in the limit of approaching zero frequency, as shown in ref 12.

When DFT is applied to large unit cells, as required for realistic periodic models of active sites for surface reactions, e.g., in zeolites, force constants have to be calculated by numerical derivatives of analytically calculated forces. Since soft, low frequency modes are characteristic of molecule−surface interactions, both the determination of the energy minimum structure and the numerical differentiation face accuracy limits when applying DFT codes designed for large scale calculations under periodic boundary conditions and using plane waves, such as VASP or CPMD. This has also been observed in previous applications of plane wave codes, e.g., in calculations of phonons for solid urea as a model of peptides.[13]

In this paper, a computational strategy is presented that improves the numerical accuracy of frequency calculations. A reoptimization step is proposed using different coordinates, normal mode coordinates instead of Cartesians. The optimization algorithm of Bouř and Keiderling[14] for optimization in normal mode coordinates has been implemented. It yields a reference structure for getting stable harmonic frequencies by numerical differentiation of forces (unavoidable for plane wave calculations on large systems) and, following, e.g., Beste[15] allows calculating anharmonic effects for each normal mode separately. As examples, the adsorption of

Received: June 28, 2013

 © XXXX American Chemical Society dx.doi.org/10.1021/ct4005504 | J. Chem. Theory Comput. XXXX, XXX, XXX−XXX

methane, ethane, and propane at the acidic sites of the zeolite chabazite (H−CHA) are considered. Adsorption in zeolites represents a challenging case because of the low-frequency floppy modes characteristic of their aluminosilicate frameworks.[7−9] The latter may couple to the low-frequency modes that are typical for molecule−surface interactions as hindered rotations or translations of the adsorbed molecule relative to the surface.

An additional advantage of the above computational scheme is that it allows a first guess of anharmonicity effects without much additional computational work. The information at the distorted structures is used to fit a polynomial potential which is used to calculate anharmonic frequencies for decoupled oscillators.[15]

METHODS

Optimization in Normal Mode Coordinates. Due to the limited accuracy of energy and gradient calculations mentioned in the Introduction, structural minimization using Cartesian coordinates to displace the atoms toward a minimal energy configuration is usually limited to loose optimization criteria (energy and/or gradient difference). For floppy structures, it is often impossible to find a minimum with very tight optimization criteria and the energy of the system oscillates around the stationary point value. A way to achieve better accuracy and therefore be able to use a tighter optimization parameter is to transform the set of atomic coordinates from Cartesian to normal mode coordinates.

The method designed by Bouř and Keiderling[14] is adopted. For a generic molecular system, the vibrational Hamiltonian can be written in harmonic approximation as

$$H = \frac{1}{2}(\mathbf{\Delta\dot{x}}^{\mathrm{T}}\mathbf{M}\mathbf{\Delta\dot{x}} + \mathbf{\Delta x}^{\mathrm{T}}\mathbf{H}\mathbf{\Delta x}) \tag{1}$$

where $\mathbf{\Delta x}$ is the vector of the atomic displacements from the equilibrium position, $\mathbf{M}$ is the diagonal matrix of atomic masses ($M_{ij} = \delta_{ij}m_i$), and $\mathbf{H}$ is the energy Hessian matrix, i.e., harmonic force constant matrix. Index i goes from 1 to $3N$ counting each Cartesian $\{x, y, z\}$ degree of freedom per atom. As common practice to remove the direct Hamiltonian dependence on the atomic masses, the Cartesian coordinates are transformed into mass-weighted coordinates $q_i = (m_i)^{1/2}\Delta x_i$ defining the transformation matrix $\mathbf{B} = \delta\mathbf{q}/\delta\mathbf{\Delta x}$, where $B_{ij} = \delta_{ij}(m_i)^{1/2}$. The coordinates and Hessian matrix are thus transformed as

$$\mathbf{q} = \mathbf{B\Delta x},\ \mathbf{f} = \mathbf{B}^{-1}\mathbf{H}\mathbf{B}^{-1} \tag{2}$$

The resulting Hamiltonian is then

$$H = \frac{1}{2}(\dot{\mathbf{q}}^{\mathrm{T}}\dot{\mathbf{q}} + \mathbf{q}^{\mathrm{T}}\mathbf{f}\mathbf{q}) \tag{3}$$

Now a linear transformation can be introduced to define normal mode coordinates as a linear combination of mass-weighted coordinates

$$\mathbf{Q} = \mathbf{s}^{\mathrm{T}}\mathbf{q} \tag{4}$$

imposing the orthogonality of the matrix $\mathbf{s}$ and requiring the similarity transformation of the Hessian

$$\mathbf{s}^{\mathrm{T}}\mathbf{s} = 1,\ \mathbf{s}^{\mathrm{T}}\mathbf{f}\mathbf{s} = \mathbf{F}, \quad \text{where } F_{ij} = \delta_{ij}\omega_i^{\,2} \tag{5}$$

The Hamiltonian can be written in diagonal from

$$H = \sum_{i=1}^{3N} \frac{1}{2}(\dot{Q}_i^{\,2} + \omega_i^{\,2}Q_i) \tag{6}$$

Thus, a linear transformation between Cartesian and normal mode coordinates is defined

$$\mathbf{\Delta x} = \mathbf{B}^{-1}\mathbf{q} = \mathbf{B}^{-1}\mathbf{s}\mathbf{Q} = \mathbf{S}\mathbf{Q} \tag{7}$$

The resulting transformation matrix $\mathbf{S}$ is a matrix of eigenvectors $[\mathbf{v}_1, \mathbf{v}_2, ..., \mathbf{v}_{3N}]$ where each column corresponds to the Cartesian coefficients of the linear combination for the kth normal mode. Thus, it is possible to displace the atoms along a specific normal mode independently.

Once the transformation is known, it can be used to perform the optimization. Bouř and Keiderling explain in detail their algorithm in a pseudocode representation.[14] Here some of the basic features of the implemented method are pointed out. The step is calculated using the rational function optimization (RFO) method[16] as

$$dQ_i^{\,\mathrm{new}} = -\frac{2g_{Q,i}^{\mathrm{old}}}{F_{ii} + \sqrt{F_{ii}^{\,2} + 4(g_{Q,i}^{\mathrm{old}})^2}} \tag{8}$$

where $\mathbf{g}_{\mathbf{Q}} = \mathbf{S}^{\mathrm{T}}\mathbf{g}_{\mathbf{x}}$ is the gradient in normal mode coordinates. A new set of Cartesian coordinates is obtained as

$$\mathbf{x}^{\mathrm{new}} = \mathbf{x}^{\mathrm{old}} + \mathbf{S}\mathbf{d}\mathbf{Q}^{\mathrm{new}} \tag{9}$$

Since at each time the coordinates change also the second derivatives of the energy do, the Hessian matrix is updated using the Broyden−Fletcher−Goldfarb−Shanno (BFGS) formula[17] in this case which ensures the Hessian to be positive defined. In case the stationary point of interest would be a first order saddle point (i.e., a transition structure), other update schemes such as the Davidon−Fletcher−Powell (DFP) method[18] can be employed. Hessian update changes consequently the eigenvalues and eigenvectors defining relatively the entity of the optimization step and its direction. This is therefore a crucial and delicate point of the algorithm.

A Hessian matrix is needed from the beginning in order to define the coordinate transformation from Cartesian to normal mode (eq 8). In this work, the starting Hessian matrix is calculated numerically for the initially optimized structures and subsequently used as an initial guess to obtain the first eigenvalues and eigenvectors for the normal mode optimization. Prior to diagonalization, the Hessian matrix is projected to remove translational and/or rotational motions of the moving frame following the usual Eckart conditions.[19]

Numerical Hessian in Normal Mode Coordinates. The intermediate step is the calculation of the harmonic frequencies of the refined structures. The most relevant source of error is the calculation of the harmonic frequencies via numerical differentiation of the gradients. The numerical error can be reduced by choosing a proper atomic displacement to sample the PES. The best choice is again a transformation from Cartesian to normal mode displacements in order to calculate directly energy and gradients along the coordinates in which the oscillations take place. From the structures optimized with the method described in the previous subsection, a further Hessian matrix in Cartesian coordinates has to be calculated in order to obtain new eigenvalues and eigenvectors (normal modes). Once the new $\mathbf{S}$ transformation matrix (eq 7) is obtained, Cartesian displacements can be performed along each normal mode independently. Similarly to eq 9, the equilibrium

dx.doi.org/10.1021/ct4005504 | J. Chem. Theory Comput. XXXX, XXX, XXX−XXX

structure $\mathbf{x}_0$ can be distorted along each normal mode individually in a positive or negative direction

$$\mathbf{x}_k^{\pm} = \mathbf{x}_0 \pm dQ_k^{\text{disp}}\mathbf{v}_k \tag{10}$$

where dQ_k^{disp} is the kth element of the normal mode displacement vector $\mathbf{dQ}^{\text{disp}}$. The values dQ_k^{disp} are chosen such that the energy difference (ΔV) related to the coordinate shift from $\mathbf{x}_0$ to $\mathbf{x}_k^{\pm}$ is always the same for all modes assuming a parabolic (harmonic) behavior of the potential (see the Supporting Information):

$$dQ_k^{\text{disp}} = \sqrt{\frac{2\Delta V}{F_{kk}}} = \frac{\sqrt{2\Delta V}}{\omega_k} \tag{11}$$

A single point calculation is performed at each $\mathbf{x}_k^{\pm}$ configuration, yielding a change in energy and gradient. Since in the basis of normal modes $\{Q_k\}$ the Hessian matrix is diagonal (eq 6), each eigenvalue can be calculated independently. Using a central two-point formula[20]

$$f' = \frac{f(x+h) - f(x-h)}{2h} \tag{12}$$

second derivatives of energy are calculated as first derivatives of the gradients. Normal mode gradients are related to Cartesian gradients via the transformation $\mathbf{g}_Q = \mathbf{s}^T\mathbf{B}^{-1}\mathbf{g}_x$. In practice, the calculation of second derivatives is performed by displacing the atoms along every normal mode (directional derivative) and each single diagonal element of the matrix $\mathbf{F}$ is given by

$$F_{kk} = \frac{\sum_{ij}\left(s_{ik}B_{ij}^{-1}g_{x_k,i}^{+} - s_{ik}B_{ij}^{-1}g_{x_k,i}^{-}\right)}{2dQ_k^{\text{disp}}} \tag{13}$$

where $\mathbf{g}_{x_k i}^{\pm}$ are the Cartesian gradients of the positive and negative displacement along the kth normal mode. These diagonal elements of the Hessian matrix $\mathbf{F}$ are related to the vibrational frequencies through $\nu_k = \omega_k/2\pi = (F_{kk})^{1/2}/2\pi$. Expression 13 can be easily extended to more than two points following the scheme proposed by Fornberg.[20] Further technical details of the method can be found in the Supporting Information.

Anharmonicity. As mentioned in the Introduction, the harmonic approximation faces limits especially when treating *soft modes*. To calculate diagonal anharmonic corrections to harmonic frequencies, the procedure implemented before by Beste[15] is adopted. The method is variational and solves the Schrödinger equation for a fourth order potential in a basis of harmonic functions for all the normal modes independently. The Hamiltonian for the kth mode is

$$H = -\frac{\hbar^2}{2}\frac{d^2}{dQ_k^{\,2}} + a_0 + a_1Q_k + a_2Q_k^{\,2} + a_3Q_k^{\,3} + a_4Q_k^{\,4} \tag{14}$$

with Q_k being the normal coordinate of the mode and a_i (i = 0, 4) the polynomial fitting coefficients of the potential. The elements of the Hamiltonian matrix are given by

$$H_{mn} = \langle\phi_m|H|\phi_n\rangle \tag{15}$$

The harmonic functions ϕ_m are solutions of the one-dimensional quantum harmonic oscillator

$$\phi_m = \sqrt{\frac{1}{2^m m!}}\left(\frac{\omega_k}{\pi\hbar}\right)^{1/4} e^{-(\omega_k/2\hbar)Q_k^{\,2}}\mathcal{H}_m\left(\sqrt{\frac{\omega_k}{\hbar}}Q_k^{\,2}\right) \tag{16}$$

where m = 0, 1, ... and $\mathcal{H}_m$ is the mth order Hermite polynomial. After application of Hermite polynomial rules to the integral of eq 15, the matrix elements can be derived analytically (see the Supporting Information).

Diagonalization of the Hamiltonian matrix for a certain number of harmonic basis functions yields the eigenvalues ϵ_i of the energy states of the anharmonic oscillator. The convergence of the quantum anharmonic vibrational partition function, calculated as an approximated sum over the states

$$q_a = \sum_{i=0}^{\infty} e^{\epsilon_i/k_BT} \approx \sum_{i=0}^{m} e^{\epsilon_i/k_BT} \tag{17}$$

with respect of the number of states given by the number of harmonic oscillator functions ($\Delta q_a = q_a^m - q_a^{m-1} < \sigma$, where σ is a reasonably small number), is used as a variational criterion. When converged, the energy states are used to calculated internal energies and entropies from the direct sum over states (see the Supporting Information). Convergence obviously depends on temperature. This work refers to standard conditions, whereas significantly higher reaction temperatures will be considered in a forthcoming study of rate constants. Fundamental anharmonic frequencies are obtained as $\nu_a = (\epsilon_1 - \epsilon_0)/h$ (where h here is Planck's constant).

Summary. To summarize, the computational protocol proposed in this work consists of the following steps:

1. Structure preoptimization in Cartesian coordinates using the standard conjugate gradient algorithm.
2. Frequency analysis from harmonic force constants obtained by numerical differentiation in Cartesian coordinates.
3. Structure refinement using normal coordinates and the optimization algorithm of Bouř and Keiderling.[14]
4. Cartesian numerical vibrational analysis of the refined structures (if imaginary frequencies are still present, step 3 is reiterated).
5. Improved harmonic frequencies by numerical differentiation of gradients using distortions along the normal mode of step 4.
6. Diagonal quantum anharmonic correction.
7. Calculation of thermodynamic functions in harmonic approximation and after anharmonic corrections.

Computational Details. Optimization in normal mode coordinates was implemented in the program EIGEN_OPT. Calculation of harmonic frequencies in normal mode coordinates and fit of the PES to a fourth order polynomial was implemented in the program EIGEN_HESS_ANHARM. Both programs are written in F90 and interface with VASP[21] in order to get total energies and gradients from single point calculations and Hessian matrix to get frequencies and corresponding eigenvectors. Each single point has been performed using a 600 eV energy cutoff at the Γ-point only requiring an energy difference between two consecutive SCF cycles of 10^{-8} eV/cell. The PBE[22] functional has been employed using Grimme's parameters[23] to include dispersion interactions.[24] Thermodynamic properties such as translational, rotational, harmonic, and anharmonic energy and entropy contributions were obtained using the local F90 program THERMO.

Methane, ethane, and propane molecules have been put in a cubic cell of 15 × 15 × 15 Å^3 and preoptimized using the VASP conjugate gradients algorithm converging the gradients up to

dx.doi.org/10.1021/ct4005504 | J. Chem. Theory Comput. XXXX, XXX, XXX−XXX

10^{-4} eV/Å. The Hessian matrix has been calculated for each structure using Cartesian central displacements providing the initial guess for the eigenvectors to be used in the normal mode optimization. Since the sampling of the energy is more accurate using normal mode coordinates, it has been possible to converge the gradients up to 10^{-6} eV/Å. In the case of unloaded H−CHA and adsorption complexes, the strucutres have been preoptimized using the conjugate gradient algorithm implemented in VASP and refined using optimization in normal coordinates as in the case of alkane molecules. The structure of interest is a 2*a* monoclinic supercell of acidic chabazite (a = 18.9033 Å, b = 9.4407 Å, c = 9.2858, α = 94.0051°, β = 94.8903°, γ = 95.3793°) with a Al/Si ratio of 1/11 (cf. Figure 1). The acidic hydrogen is located at the O2 position following the work of Bučko et al.[25]

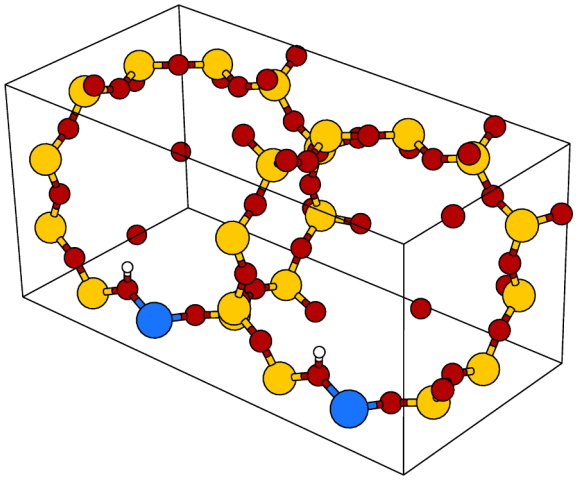

Figure 1. H−CHA 2*a* supercell showing the acidic hydrogens in position O2 (oxygen shared by two eight-membered rings and one four-membered ring).

RESULTS AND DISCUSSION

Optimized Structures. *Small Alkane Molecules.* First, the three small molecules of interest for the adsorption studies have been considered. Structural optimization in normal mode coordinates leads to lower energy structures (see the Supporting Information for optimization energy profiles).

It is no surprise that for methane and ethane the effect of structure refinement is rather small in the energy, whereas for propane the change is noticeable (~0.19 kJ/mol). It mainly arises from the optimization of the different hindered rotor modes which, due to the flatness of the potential energy surface, cannot be accurately minimized using common Cartesian coordinates. While the energy minimization converges after very few steps, the gradients (considered in this study as the only criterion to stop the minimization process) take more steps. This feature can be ascribed to two possible opposite driving forces. While the gradient is a vector quantity and contains much more detailed information, it suffers, for the same reason, from more numerical noise. On the other hand, the energy is a scalar with averaged information and therefore the noise is more systematic, resulting in a faster convergence of this parameter during the optimization.

H−CHA and Adsorption Structures. The accurate determination of the adsorption structures of molecules at a catalytic site is a challenging goal in the field of theoretical catalysis. One of the main structural features of zeolites is the floppiness of their lattices. This makes zeolites very susceptible to external perturbations such as molecules entering the cavity. Therefore, the optimization of such structures, involving floppy motions of the zeolite framework and low frequency motions (*hindered* translations and rotations relative to the framework) of the adsorbed molecules,[11] can be difficult.

Once a reference structure has been preoptimized using standard Cartesian optimization methods, a more accurate minimization can be applied in order to refine the structure.

In Figure 2, the energy minimization profiles for the adsorption structures of methane, ethane, and propane at the catalytic OH group are reported.

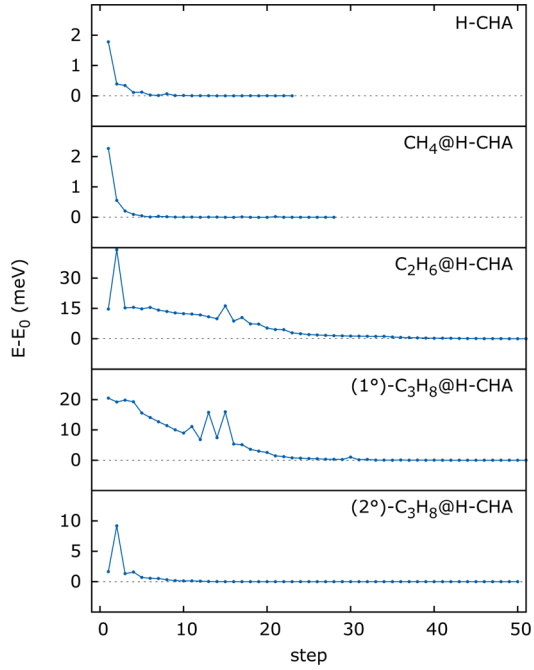

Figure 2. Energy minimization profile for structure refinement using optimization in normal mode coordinates. Unloaded H−CHA and its adsorption complexes with methane, ethane, and propane adsorbed via primary (1°) and secondary carbon (2°).

The effect on the energy of the optimization in normal coordinates is much more evident. While for unloaded H−CHA and for the methane adsorption complex the optimization leads to a simple structural relaxation, with the energy smoothly converging, in the other cases a local rearrangement is taking place. The "bumps" in the profiles at the beginning of the minimizations indicate substantial structural changes. This fact shows that the optimization scheme, exploring the local PES, is able to find more stable configurations. This is not surprising, since the implemented algorithm uses the RFO approach[16] to calculate the steps allowing the search for other stationary points in the neighboring region and supplying a better description of the local PES through a [2/2] Padé approximant. This is a major improvement in such anharmonic regions.

Figure 3 shows the adsorption complexes. As a common structural motif, the acidic hydrogen in the O2 position points toward the carbon atom, extending its coordination sphere by a fifth hydrogen atom, however at a much larger distance. Table 1 reports the most relevant interatomic distances (r_1 ($r_{C\cdots H(O)}$), r_2 ($r_{(C)H\cdots O}$)). Using the method proposed here, the local

dx.doi.org/10.1021/ct4005504 | J. Chem. Theory Comput. XXXX, XXX, XXX−XXX

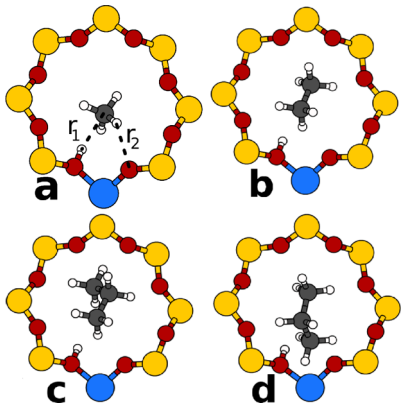

Figure 3. Adsorption complexes of (a) methane, (b) ethane, (c) propane via primary carbon, and (d) propane via secondary carbon with the acidic group at HO2 in an eight-membered ring of H−CHA.

Table 1. Relevant Bond Distances (pm) for Adsorption Complexes

	PBE+D (this work)		PBE+D[26]	PW91[25]	
alkane	r_1	r_2	r_1	r_1	r_2
methane	215	256	212	247	364
ethane	214	273	236	235	252
propane (C(1°))[a]	213	264	238	240	252
propane (C(2°))[b]	218	264		251	255

[a]Propane adsorbed via primary carbon to hydroxyl group. [b]Propane adsorbed via secondary carbon to hydroxyl group.

coordination of the alkane does not change much depending on the carbon number. This is expected, since the methyl and ethyl groups of adsorbed ethane and propane are not involved in the specific interaction of the methyl group with the surface OH group. This feature was not observed in previous calculations using standard optimization techniques with Cartesian coordinates.[25,26]

As for alkanes in the gas phase, the energy converges faster compared to the gradients which, due to even more pronounced inaccuracies (intermolecular long-range interactions, etc.), are in this case much more noisy. Comparison of the electronic adsorption energies (Table 2) shows a rather small but general stabilization of the adsorption complexes whose structures have been refined by reoptimization in normal coordinates. If the absolute energies are taken into account, it is clear that the structural changes are extremely relevant. It will be shown below how the frequencies and thus the vibrational energies are affected by changes of the reference structures.

Table 2. Electronic PBE+D Energies, ΔE_e in kJ/mol, for Adsorption of Alkanes in H−CHA (θ = 0.5)[a]

optimization coordinates	normal mode	Cartesian	Cartesian	
alkane	PBE+D, this work		PBE+D, ref 26	PW91, ref 25
methane	−34.77	−34.72	−32.32	−11
ethane	−47.02	−45.78	−43.42	−10
propane (C(1°))[b]	−58.89	−57.32	−59.44	−15
propane (C(2°))[c]	−58.04	−58.30		−11

[a]Re-optimization in normal mode coordinates vs optimization in Cartesian coordinates. [b]Propane adsorbed via primary carbon to hydroxyl group. [c]Propane adsorbed via secondary carbon to hydroxyl group.

Frequency Analysis and Anharmonic Corrections. To get more accurate frequencies, another harmonic analysis has to be performed for the refined structures (see the Supporting Information). Since the frequencies related to the *soft modes* contribute at most to the vibrational entropy but are also most affected by numerical errors, symmetric eight-point displacements have been performed along modes with frequencies lower than 300 cm^{-1}. The sampling procedure allows at the same time to fit the potential. For the higher frequencies, the inclusion of anharmonicity is less important in terms of orders of magnitude and the numerical noise affecting the energy is negligible. Thus, for such vibrations, a two-point displacement is sufficiently accurate.

Figure 4 illustrates how the use of more points in the numerical differentiation enhances the accuracy of the calculated frequencies. It shows the ratios of the frequencies calculated with two, four, and six points with respect to the eight-point frequencies (considered as the best estimate) for the *soft modes* region of the unloaded H−CHA. The frequency sets are converging while the number of points grows. The limit of eight points displaced along each normal mode can be considered reasonably accurate. It must be pointed out that this is the accurate harmonic value for the given potential energy surface, obtained, e.g., by PW-DFT or PBE+D, which is not necessarily close to the experimental value. It rather means that the errors associated to the numerical noise become progressively negligible.

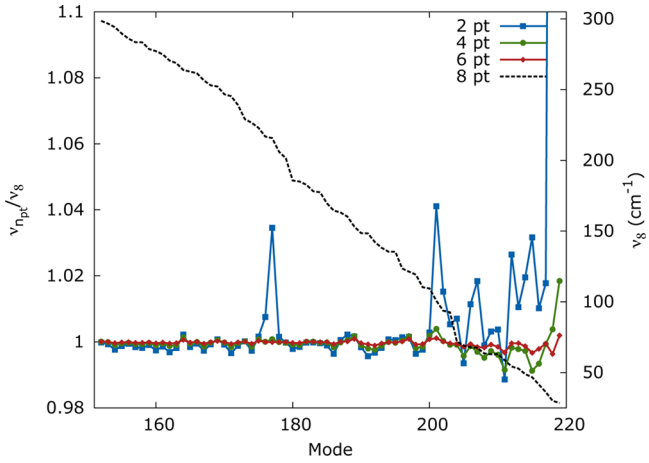

Figure 4. Ratios between numerical frequencies calculated with two-, four-, and six-point formulas and a reference set of frequencies (---) calculated with an eight-point formula for the vibrations lower than 300 cm^{-1} in unloaded H−CHA.

From the same frequency calculations, the quartic order fit to include anharmonicity has been obtained for each normal mode. For each vibration, the variational approach described above has been applied using a convergence parameter $\sigma = 10^{-4}$ at a given temperature. Individual contributions to the vibrational energy and entropy have been added from the sum over states formula (eq 17). In Table 3, the thermodynamic properties for small alkanes adsorption on H−CHA are reported. The comparison is made between the results of a Cartesian harmonic analysis at structures optimized using a conjugate gradients algorithm provided by VASP and Cartesian harmonic (ν_{Cart}), normal mode harmonic (ν_{NM}), and

dx.doi.org/10.1021/ct4005504 | J. Chem. Theory Comput. XXXX, XXX, XXX−XXX

Table 3. Zero Point Vibrational Energies, ΔE_{ZPV}, Internal Energies, ΔE, Enthalpies, ΔH, Gibbs Free Energies, ΔG, Entropy Contributions to the Latter, $-T\Delta S$, and Vibrational Entropies Only, $-T\Delta S_{vib}$, for Adsorption of Alkanes in H−CHA at Standard Conditions (273.15 K, 0.1 MPa, θ = 0.5) All in kJ/mol

	ΔE_{ZPV}				$\Delta E_{273.15}$			
	Cartesian	normal modes			Cartesian	normal modes		
	ν_{Cart}	ν_{Cart}	ν_{NM}	ν_{Anharm}	ν_{Cart}	ν_{Cart}	ν_{NM}	ν_{Anharm}
methane	4.25	4.01	4.79	4.01	−27.15	−29.35	−28.17	−33.29
ethane	3.23	1.49	3.94	2.13	−39.11	−40.12	−39.72	−45.64
propane (C(1°))[a]	2.25	2.06	2.35	2.56	−50.23	−54.82	−52.10	−53.79
propane (C(2°))[b]	2.03	2.67	1.72	0.75	−51.61	−54.50	−52.05	−54.74
	$\Delta H_{273.15}$				$\Delta G_{273.15}$			
	Cartesian	normal modes			Cartesian	normal modes		
	ν_{Cart}	ν_{Cart}	ν_{NM}	ν_{Anharm}	ν_{Cart}	ν_{Cart}	ν_{NM}	ν_{Anharm}
methane	−29.44	−31.63	−30.44	−35.56	5.29	−2.28	−0.25	4.28
ethane	−41.39	−42.38	−41.99	−47.99	−10.25	−9.22	−5.95	−0.93
propane (C(1°))[a]	−52.51	−57.09	−54.37	−56.06	−13.89	−20.03	−17.31	−12.72
propane (C(2°))[b]	−53.89	−56.77	−54.32	−57.01	−9.67	−18.59	−16.22	−13.17
	$-T\Delta S_{273.15}$				$-T\Delta S_{vib,273.15}$			
	Cartesian	normal modes			Cartesian	normal modes		
	ν_{Cart}	ν_{Cart}	ν_{NM}	ν_{Anharm}	ν_{Cart}	ν_{Cart}	ν_{NM}	ν_{Anharm}
methane	34.73	29.34	30.18	39.84	−15.27	−20.66	−19.82	−10.16
ethane	31.14	33.17	36.03	46.97	−28.04	−26.01	−23.14	−12.20
propane (C(1°))[a]	38.62	37.05	37.06	43.34	−27.59	−29.16	−29.14	−22.86
propane (C(2°))[b]	44.22	38.18	38.09	43.84	−21.99	−28.03	−28.11	−22.36

[a]Propane adsorbed via primary carbon to hydroxyl group. [b]Propane adsorbed via secondary carbon to hydroxyl group.

anharmonic (ν_{Anharm}) frequencies results at the refined structures optimized using normal mode coordinates. In Table 4, the adsorption equilibrium (Henry) constants (K_{ads})

Table 4. Adsorption Equilibrium (Henry) Constants and Half Coverage Pressure (MPa) for a Langmuir Model

alkane	K_{ads}	$p_{1/2}$
methane	0.151	0.658335
ethane	1.506	0.066398
propane (C(1°))[a]	270.641	0.000369
propane (C(2°))[b]	329.948	0.000303

[a]Propane adsorbed via primary carbon to hydroxyl group. [b]Propane adsorbed via secondary carbon to hydroxyl group.

and half coverage pressure ($p_{1/2}$) for a Langmuir model[27] are reported for the data obtained from the anharmonic free energies of adsorption.

Comparing first the results of the Cartesian harmonic analysis, it is seen that the reference structure influences not only the electronic energy of the system but induces substantial differences to the vibrational structure. Considerable variations in the internal energies and vibrational entropies are observed which are not only due to changes of the electronic stabilization. Moreover, the structures refined with the normal mode optimization present a monotonic decrease of the vibrational entropies, a feature not shown by the Cartesian optimized ones. Such a behavior which is in accord with experimental trends (*vide infra*) is a clear indication that a better accuracy of the vibrational contributions is reached. From the anharmonic frequency results at the normal mode optimized structures, further conclusions can be drawn. Remember that the anharmonic corrections have been applied only for the *soft mode* region. The quantity that is clearly changing more evidently is the vibrational entropy which is known to be extremely sensitive to changes in low frequency values. No substantial changes occur between the normal mode and the Cartesian numerical frequencies results, while the inclusion of anharmonicity leads to a completely different estimate of the vibrational entropy and therefore of the Gibbs free energy. To identify the origin of these differences in Figure 5, the differences between anharmonic vs harmonic results for the single oscillator contributions to the vibrational entropy are plotted for each normal mode for $\nu_i \leq 300$ cm^{-1}. The plots show that for most of the normal modes the two different contributions to the total vibrational entropy are not very different. Just for some specific normal modes the anharmonic contribution is much lower than the harmonic one. This feature is more pronounced in the case of adsorbed molecules. It can be mainly ascribed to two adsorption related phenomena, the rigid body motions (hindered rotations and translations[11]) of the molecule with respect to the crystal framework and the influence of the adsorbed molecules on the framework vibrations. The coupling of both of them gives rise to significant anharmonic deviations. Thus, since the anharmonic effects are not influencing considerably the vibrational entropy of the unloaded H−CHA and of the gas-phase molecules, the total vibrational entropy is lower, yielding higher Gibbs free energies and therefore making the adsorption complexes thermodynamically less stable.

Comparison with Experiments and Simple Adsorption Models. For alkane adsorption on H−CHA, the only work reporting thermodynamic data at standard conditions is that of Barrer and Davies.[28] The H−CHA sample used in that study has a much higher aluminum content Al/Si ∼ 1/3 than the model employed in this work (Al/Si = 1/11), resulting in a very high concentration of active sites per unit cell.

dx.doi.org/10.1021/ct4005504 | J. Chem. Theory Comput. XXXX, XXX, XXX−XXX

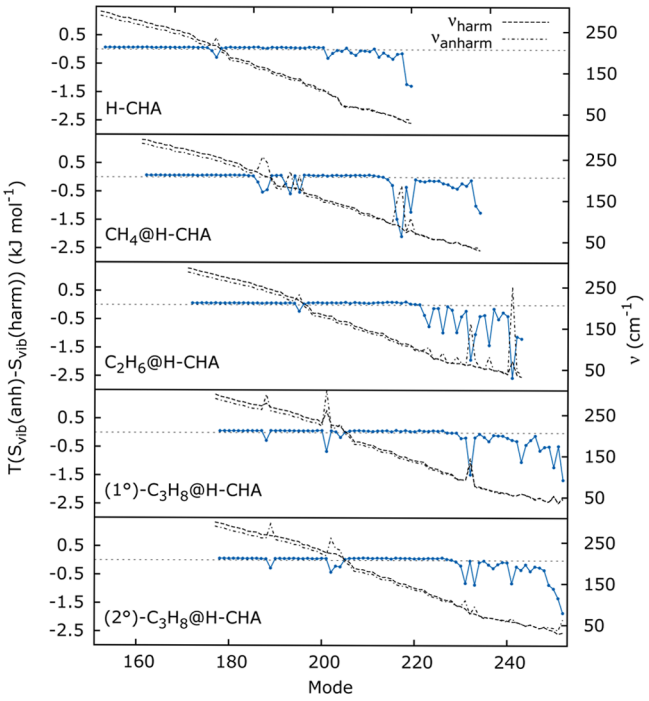

Figure 5. Differences between anharmonic and harmonic single oscillator contribution to the vibrational entropy at 273.15 K (blue dots, left scale) for the unloaded H−CHA and for the adsorption complexes with methane, ethane, and propane (adsorbed via primary (1°) and secondary carbon (2°)). The black lines show the absolute harmonic (−−−) and anharmonic (−·−) frequencies (right scale). Only the modes are listed for which anharmonic correction has been calculated.

Comparison is also made with the results of simple adsorption models. On adsorption, a molecule loses its translational and rotational degrees of freedom and vibrates relative to the surface. Since the binding of the molecule to the surface is of van der Waals type, the potential energy surface for most of these degrees of freedom will be flat and some vibrations of the molecule will still conserve part of the translational and rotational character of the gas phase molecule. Taking this into account, several models have been proposed[29,30] to calculate entropies for molecule−surface interactions. For example, for H_2 adsorption in metal−organic frameworks,[31] the assumption has been made that the molecule is freely rotating on the surface. Following the method proposed by Tait et al.[29] for the desorption of linear alkanes from the MgO(100) surface, the Gibbs free energies have been calculated for an immobile adsorbate model, where no translations or rotations are allowed in the adsorbed state, for a rotating adsorbate, where only rotations along the adsorbate principal axis of inertia are allowed, and for a mobile adsorbate, where 2D translations and some specific rotations are allowed depending on the nature of the molecule (for more detailed information, see ref 29). Table 5 summarizes the treatment of the various degrees of freedom.

In Figure 6, Gibbs free energies of adsorption calculated using standard Cartesian optimization and numerical differentiation, normal mode optimization, and normal mode numerical differentiation without and with anharmonic corrections are plotted together with the experimental data of Barrer and Davies[28] and the resulting energies from the simple adsorption models described above.

Table 5. Degrees of Freedom of the Adsorbate for Different Adsorption Models as Proposed by Tait et al.[29]

adsorbate model	degrees of freedom
immobile	0 Tr + 0 Rot
rotating	0 Tr + 3 Rot
mobile	2 Tr + n Rot

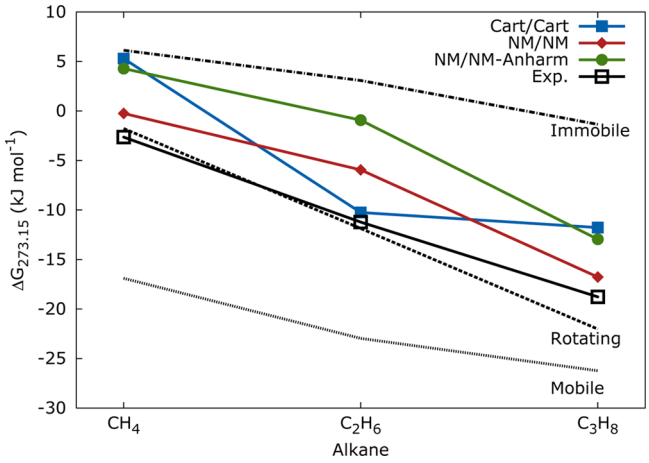

Figure 6. Adsorption Gibbs free energies for methane, ethane, and propane (averaged using Boltzmann weights for primary and secondary carbon adsorption) from different computational approaches, experiment,[28] and simplified adsorption models.

The experimental trend is reproduced by the theoretical results derived for the structures obtained with the normal mode optimization method and subsequent normal mode vibrational analysis but not by the results obtained with standard methods. Moreover, both the experimental and computational results lie in between the simplified models for adsorption, but again, only the results obtained with the proposed method resemble the decrease from methane to ethane and propane. It may seem that the inclusion of anharmonic corrections brings the computational results further away from the experimental data. However, as already mentioned, experimental data have been obtained for a system containing almost 10 times more active sites per unit cell. At full coverage, this implies the presence of many adsorbate molecules in close contact. Favorable lateral interactions between different adsorbate molecules may result in a lower Gibbs free energies of adsorption[9,32] at the given temperature. To the about 10 kJ/mol difference between experimental and computational results, apart from neglected anharmonic couplings, also the limited accuracy of PBE+D energies may contribute. Future studies will assess the effect of hybrid MP2:(DFT+D) structure optimizations and evaluate coupled cluster corrections to the binding energies; see ref 32.

CONCLUSIONS

Due to numerical accuracy limits, plane wave DFT calculations may have difficulties to tightly converge energy minimum structures for systems with flat potential energy surfaces, as indicated by oscillations of energy and structure parameters. Another indication of numerical instabilities is the presence of small imaginary frequencies when trying to characterize the stationary points as minima or saddle points. These difficulties can be overcome by a refinement optimization step in which normal mode coordinates instead of Cartesian coordinates are

dx.doi.org/10.1021/ct4005504 | J. Chem. Theory Comput. XXXX, XXX, XXX−XXX

used. Displacements in normal mode coordinates are also recommended when calculating harmonic vibrational frequencies from finite differences of energy gradients. The harmonic frequencies using central displacements along normal modes show a convergent behavior when enlarging the number of symmetrically placed points. When harmonic frequencies obtained this way are used to calculate vibrational contributions instead of frequencies obtained with Cartesian distortions after optimization in Cartesian coordinates, the free energies of adsorption of small alkanes as a function of the carbon number show a much more regular behavior in agreement with the trend of the experimental results. The change in the free energies due to the normal mode approach is not systematic and varies between +4.3 (ethane) and −6.6 kJ/mol (propane, secondary carbon). The one-dimensional polynomial fits of the potential energy surface obtained from the symmetric distortions along each normal mode can be used to get a first estimate of anharmonicity effects. They are dominated by an increase of low vibrational frequencies associated with hindered translations and rotations of the adsorbed molecules and the floppy modes of the zeolite framework. Approximate inclusion of anharmonicities leads to a systematic increase of the Gibbs free energy of adsorption of 3.1−5.0 kJ/mol, making adsorption less favorable.

■ ASSOCIATED CONTENT

Supporting Information

Solution of the anharmonic Hamiltonian, anharmonic vibrational thermodynamics functions, technical details of the normal mode numerical differentiation, and alkane minimization energy profiles. This material is available free of charge via the Internet at http://pubs.acs.org.

■ AUTHOR INFORMATION

Corresponding Author

*E-mail: js@chemie.hu-berlin.de.

Notes

The authors declare no competing financial interest.

■ ACKNOWLEDGMENTS

This work has been supported by a computer grant from the North German Computing Alliance Berlin - Hannover (HLRN) and by the “Fonds der Chemischen Industrie”. G.P. is a member of the International Max Planck Research School “Complex Surfaces in Material Sciences” and thanks the “Verband der Chemischen Industrie” for a Kekulé stipend. G.P. acknowledges Prof. M. Sierka for help in programming issues and Dr. J. Paier for reading and commenting on the manuscript.

■ REFERENCES

(1) Claeyssens, F.; Harvey, J. N.; Manby, F. R.; Mata, R. A.; Mulholland, A. J.; Ranaghan, K. E.; Schütz, M.; Thiel, S.; Thiel, W.; Werner, H.-J. *Angew. Chem., Int. Ed.* **2006**, *45*, 6856−6859.
(2) Svelle, S.; Tuma, C.; Rozanska, X.; Kerber, T.; Sauer, J. *J. Am. Chem. Soc.* **2009**, *131*, 816−825.
(3) Hansen, N.; Kerber, T.; Sauer, J.; Bell, A. T.; Keil, F. J. *J. Am. Chem. Soc.* **2010**, *132*, 11525−11538.
(4) Tuma, C.; Sauer, J. *Angew. Chem., Int. Ed.* **2005**, *44*, 4769−4771.
(5) Campbell, C. T.; Sellers, J. R. V. *J. Am. Chem. Soc.* **2012**, *134*, 18109−18115.
(6) Torrie, G.; Valleau, J. *J. Comput. Phys.* **1977**, *23*, 187−199.
(7) Straatsma, T. P.; Berendsen, H. J. C. *J. Chem. Phys.* **1988**, *89*, 5876−5886.
(8) Hobza, P.; Sauer, J.; Morgeneyer, C.; Hurych, J.; Zahradnik, R. *J. Phys. Chem.* **1981**, *85*, 4061−4067.
(9) Sillar, K.; Sauer, J. *J. Am. Chem. Soc.* **2012**, *134*, 18354−18365.
(10) De Moor, B. A.; Ghysels, A.; Reyniers, M.-F.; Van Speybroeck, V.; Waroquier, M.; Marin, G. B. *J. Chem. Theory Comput.* **2011**, *7*, 1090−1101.
(11) De Moor, B. A.; Reyniers, M.-F.; Marin, G. B. *Phys. Chem. Chem. Phys.* **2009**, *11*, 2939−2958.
(12) Cramer, C. J. *Essentials of computational chemistry: theories and models*; Wiley: England, 2004.
(13) Johnson, M.; Parlinski, K.; Natkaniec, I.; Hudson, B. *Chem. Phys.* **2003**, *291*, 53−60.
(14) Bouř, P.; Keiderling, T. A. *J. Chem. Phys.* **2002**, *117*, 4126−4132.
(15) Beste, A. *Chem. Phys. Lett.* **2010**, *493*, 200−205.
(16) Banerjee, A.; Adams, N.; Simons, J.; Shepard, R. *J. Phys. Chem.* **1985**, *89*, 52−57.
(17) Broyden, C. G. *J. Appl. Math.* **1970**, *6*, 76−90.
(18) Fletcher, R.; Powell, M. J. D. *Comput. J.* **1963**, *6*, 163−168.
(19) Eckart, C. *Phys. Rev.* **1934**, *46*, 383−387.
(20) Fornberg, B. *Math. Comput.* **1988**, *51*, 699−706.
(21) Kresse, G.; Hafner, J. *Phys. Rev. B* **1993**, *47*, 558−561.
(22) Perdew, J. P.; Chevary, J. A.; Vosko, S. H.; Jackson, K. A.; Pederson, M. R.; Singh, D. J.; Fiolhais, C. *Phys. Rev. B* **1992**, *46*, 6671.
(23) Grimme, S. *J. Comput. Chem.* **2006**, *27*, 1787−1799.
(24) Kerber, T.; Sierka, M.; Sauer, J. *J. Comput. Chem.* **2008**, *29*, 2088−2097.
(25) Bučko, T.; Benco, L.; Hafner, J.; Ángyán, J. G. *J. Catal.* **2007**, *250*, 171−183.
(26) Goltl, F.; Gruneis, A.; Bučko, T.; Hafner, J. *J. Chem. Phys.* **2012**, *137*, 114111.
(27) Sauer, J.; Ugliengo, P.; Garrone, E.; Saunders, V. R. *Chem. Rev.* **1994**, *94*, 2095−2160.
(28) Barrer, R. M.; Davies, J. A. *Proc. R. Soc. London, Ser. A* **1971**, *322*, 1−19.
(29) Tait, S. L.; Dohnalek, Z.; Campbell, C. T.; Kay, B. D. *J. Chem. Phys.* **2005**, *122*, 164708.
(30) De Moor, B. A.; Reyniers, M.-F.; Gobin, O. C.; Lercher, J. A.; Marin, G. B. *J. Phys. Chem. C* **2011**, *115*, 1204−1219.
(31) Sillar, K.; Hofmann, A.; Sauer, J. *J. Am. Chem. Soc.* **2009**, *131*, 4143−4150 (PMID: 19253977).
(32) Tosoni, S.; Sauer, J. *Phys. Chem. Chem. Phys.* **2010**, *12*, 14330−14340.